Original Article

Assessment of aquifer vulnerability status and groundwater management studies using integrated geophysical techniques in Ewekoro South-West Nigeria

S. A. Ishola[1] Ⓛ, V. Makinde[2], O.O. Alatise[2], H.O. Edunjobi[2], and C.O Ogunkoya[3]

Abstract

Twenty-five vertical electrical soundings and ten 2D electrical resistivity tomography profiles were undertaken at Ewekoro District in Ogun-State, Nigeria. The work encompassed the utilization of Schlumberger and Wenner Array. Subsurface profiles were obtained using Direct Current Resistivity (DCRE) of Vertical Electrical Sounding using AGI Super-sting Earth Resistivity meter with schlumberger configuration; current electrode spacing (AB/2) ranging from 1.0 to maximum of 200m and the potential electrodes (MN/2) were consequently changed from 0.25 m to 5.0 m respectively which was further complemented by application of 2D electrical resistivity tomography (ERT) adopting Wenner array of electrode spacing of 10 m for the profile length of 200 m was maintained to attain a reading and imaging within the depth range of aquifer in the area for the effective characterization of the subsurface structures and delineation of the underlying aquifer. The interpretations of acquired resistivity data were carried out with manual procedures coupled with Resist, RES2DINV and Surfer software programs for VES, 2D-ERT and contouring respectively. The results of the hydraulic conductivity (K) cum hydraulic resistance (C) for the protective layers were estimated from the geoelectrical parameters estimated have values ranging from 0.00815 cms^(-1) (VESEWE24) to 5.484 cms^(-1) (VESEWE1) and 0.0075day^(-1) (VESEWE21) to 15445.98 day^(-1) (VESEWE25) respectively. AVI rating implications revealed that the study area is dominantly characterized by Extremely High Vulnerability (EHV); most of the locations were extremely high (88%) while VESEWE23 and VESEWE24 (8%) exhibited high vulnerability status and only VESEWE25 depicted low vulnerability status (4%).

Key words: Vulnerability index; hydraulic resistance; geoelectrical parameters; tomography

---

Affiliation Info: [1] Department of Earth Sciences, Olabisi Onabanjo University Ago-Iwoye, P.M.B 2002, Ago-Iwoye, Ogun State, Nigeria; [2] Department of Physics, Federal University of Agriculture Abeokuta, P.M.B 2240, Abeokuta, Ogun State, Nigeria; [3] Department of Physics, Ajayi Crowther University, Oyo Oyo, Oyo State, Nigeria.

Corresponding AurhorⓁ: Ishola, S.A. PhD, Exploration Geophysics and Geomathematics; Email: ishola.sakirudeen@oouagoiwoye.edu.ng.

Citation: Ishola, SA; Makinde, V; Alatise, OO; Edunjobi, HO and Ogunkoya, CO. 2025. Assessment of aquifer vulnerability status and groundwater management studies using integrated geophysical techniques in Ewekoro South-West Nigeria. *Naturalis Scientias*, 2 (2): 549-573. DOI: https://doi.org/10.62252/NSS.2025.1033. www.naturalisscientias.com.

---

1. Introduction

Groundwater found beneath the water table and within the zone of saturation responds to movement and follow the same direction with the sloping of the water table and encompasses the moisture located in the pore spaces in the rock matrix. Obtaining clean and portable water for domestic, industrial and overall usage is a fundamental necessity for household usage and socio-economic development. The basic information obtainable from the controlling force of nature and corresponding geology of subsurface status at any given point in time is very significant in groundwater exploration and development. For efficient maintenance, sustenance and ultimate utilization of groundwater resources for the benefits of all and sundry; adequate protection and effective management of buried aquifers with thick overlying sediments is therefore necessary[1-4]. Seepages of surface pollutants emanating from local environment ranging dumpsites, sewage system and run-off are some of the terrain activities that can the quality of groundwater[5-6]. Migration of these pollutants into the groundwater table can have unprecedented impacts on the groundwater thereby affecting its potability[7-9]. The seepages of these pollutants is greatly enhanced as a result of highly permeable overlying layers of the subsurface coupled with the ease at the contaminant fluid flows through the subsurface as the fluid flow is a function of combination of certain hydrogeological features namely intergranular pores, faults, fissures and fractures that are somewhat interconnected. In order to demystify several hydrogeological and hydrological problems, the significance of quantitative description of aquiferous zones cannot be overemphasized[10].

The background knowledge of aquifer characterization and vulnerability studies of the groundwater system is highly expected for effective shielding of the groundwater system from external invasions. Vulnerability of aquifer is a reflection of the strength of the subsurface characteristics; whether they are capable enough to prevent or favour the transportation and consequent migration of the contaminant seepages into the aquifer repositories. Also, the vulnerability of any aquifer system is dependent on groundwater flow whose corresponding velocity (groundwater flow velocity) thereby enhances it; a factor that is very much dependent on both the water table depth as well as the hydraulic conductivity overlying the concerned aquifer. Furthermore, for effective groundwater protection, the overlying cum protective layers must possess a reasonably high thickness with associated low hydraulic conductivity. When the period of percolation exceeded ten years, it is considered necessary as suggested by[11] while the presence of abundant intrusions or fissures that are typically of sandy sediments can create pathways for percolation and subsequent migration of contaminant seepages within the protective layers but oftentimes, this inhomogeneous condition of the subsurface are not taken into proper consideration in groundwater studies[1-4].

Once the sanitary integrity is affected, it can result to various illnesses of water-borne origin which can also affect human health and biological population. This may in one way or the other jeopardize the day to day economic engagement and other associated activities in the area[12].

The vertical electrical sounding (VES) and electrical resistivity tomography (ERT) methods have been profitably applied by numerous researchers and consequently documented and published in literatures in the field of geophysics and groundwater exploration studies in resolving clusters of hydrogeological and hydrogeophysical challenges which includes

delineation of depth to water table, saturated aquifer horizons mapping, aquifer characterization and groundwater development studies, evaluations of rate of vadose zone infiltrations as well as in overall groundwater contamination studies[13-16]. The techniques are highly preferable since the resistivity contrast can be obtained when the aquiferous zones are attained[17-21]. The conductivity/resistivity of the arenaceous or argillaceous geological formations are displayed by the integration of VES and ERT as they are respectively distributed both vertically and laterally thereby serving as a good correlation tool for effective detection and subsequent delineation of aquiferous zone[22-23]). The daily increase in human and biological population and general quest water in numerous communities have led to increased agitations for groundwater coupled with unavailability and doubtful quality of available surface water. Most of the boreholes earlier drilled without preliminary professional investigations have failed due borehole collapse and water contamination thereby rendering these boreholes as abandoned wells.

As part of the approach undertaking to salvage these aforementioned problems, the factors contributing to water scarcity and impairment of available water by lithology and local geology have to be evaluated and independently addressed in an area under investigation. The controlling forces governing aquifer condition are reflections of the inherent compositions of the subsurface which play significant roles in assessing groundwater flow from the surface to the subsurface via several networks of recharge processes[23-24]. The adopted techniques, aside from their relative availability and easy accessibility; their capability in revealing distinctively the subsurface formations that are permeable due to unconsolidated materials and therefore permitting permeability via the infiltrating surface contaminants migrating to the subsurface[5 & 24]. The VES method is a depth sounding technique which has over the years proven to be effective while possessing a wide range of application in groundwater exploration and development studies, and ERT possesses a wide application for detailed investigative studies encompassing the overlying layers due to its inbuilt sensitivity to contrasts in lithologic unit. These two techniques have proven to be of high reliability measures in aquifer studies and the accompanied software packages that are readily available for post field data processing, analyses and subsequent interpretation of acquired data make them veritable tools in overall groundwater studies. The application of these non-invasive techniques in determining aquifer characteristics encompasses the acquisition, processing, analysis and consequent interpretation of the local hydrogeological conditions for the ease of evaluating aquifer potential evaluations and determination of geohydraulic properties of any given area. Furthermore, the integration of the aquifer vulnerability index (AVI) functions as a complementary evaluation tool whether the overburden layer is shielded from the external contaminant seepages emanating from the surface and estimating the level of protection if it is, if it is will go a long way in demonstrating the effectiveness of these methods. The principal goal of this study was accomplished via the following stated predetermined objectives: determining the depth and corresponding thickness of each geoelectrical layers for the purpose of estimating the geohydraulic parameters of the formation which in turn leads to effective and procedural assessment of the vulnerability index of the protective layers of the aquifer thereby proposing the most effective and economical class of exploration and management techniques for the study area's groundwater system.

2. Study area

2.1 Location and geological setting

Ewekoro community in Ogun State serves as one out of the numerous mills of West African Portland Cement Company (WAPCO) and Dangote group Cement Company. It is a sleepy neighbouring town with close proximity to Papalanto, a town predominantly recognized for sugarcane plantation. It is found between latitude 6˚53˙ N and longitude 3˚14˙ E[25]. Ewekoro formation and Abeokuta formation are geologically part of the sedimentary rocks of Ogun State. Ewekoro subsurface geology is highly fossiliferous and consisting of deposits of limestones being daily quarried by WAPCO for economic purposes[23]. The cement manufacturing facility situated in Ewekoro is located 5 kilometres north of Ewekoro town (6°55˙ N and 3°12˙ E). Also, this location is calculated to be of 64 kilometers north of Lagos and 42 kilometers south of Abeokuta on the approximate respective distance and is found within the tropical rainforest belt of Nigeria. Olapeleke community is loated in the Western side, Itori community located in the Northern side, while Elebute and Alaguntan communities both of which were jointly in the Eastern part predating the factory are located within 10 km radius of the production facility and serve as the notable farming settlements in the investigated area[21]. These aforementioned settlements are perennially drained by Itori, Ewekoro, Eshe, Elebute as well as Alaguntan Rivers where Alaguntan River is the only river directly receiving waste water migrating from the cement plant. Nevertheless, non-point pollutants from run-offs and dust deposits from the atmosphere primarily influenced the sanitary qualities of other catchment rivers. The area is characterized by particulate matters like cement dusts and other material deposits enhanced by an average wind velocity of about 1.0 and 0.72 msG around 10 m higher above the ground level during the dry (January-March) and wet seasons (May-November) respectively[21]. One of the overriding weather situations governing the catchment area of the cement plant is average relative humidity in the recorded range of 65±10% alongside average annual rainfall in the range of 1500±120 mm. Limestone composition of about 11m to 12m is found at the type locality of Ewekoro formation. The base of the formation is typically sandy grading in a downward direction into Abeokuta Formation. The Phosphatic glauconitic grey coloured shale overlain Ewekoro formation[5 & 25]. Ewekoro formation is consistent generally with the regional geology of eastern section of the Dahomey Basin; it comprises of the limestone that are not only thinly laminated fissile and probably non-fossiliferous shale as predominant rocks but are also non-crystalline and non-fossiliferous[26]. Furthermore, Ewekoro formation is comprised of intercalations sedimentary deposits of argillaceous origin; though characterized by softness and friability but equally cemented by ferruginous and siliceous materials in some places. The lithological units in Ewekoro formation are clayey sand, clay, shale, marl, limestone and sandstone[25].

The investigated area is known to range from a generally low lying to gentle steeping undulating terrain located within the humid tropical climate typified by two notable seasons distinctively predominant in the tropical region of southern Nigeria; the wet and the dry seasons. Usually, the occurrence of wet season varied from March to October where the prevailing climate is predominantly characterized by either the tropical maritime airmass

or the moisture laden Southwest winds migrating the Atlantic Ocean with heavy precipitations; large portion of the precipitations occurs in seemingly torrential downpours displaying high high run-off and sometimes flooding as the resultant effects while the occurrence of the dry season starts in November until late February or beginning of March subjected to the overriding trigger of the dry continental airmass or north-easterly winds migrating from the sahara desert. The major water bodies in the region are Yewa and Ogun rivers which flow into Lagos lagoon while their tributaries are found in Ewekoro Local Government Area as Alaguntan River, Akinbo River and Eshe River. There are however streams running parallel in the area. Also ponds are not left out. The fluctuations of the water table are in response to the seasonality of the observed rainfall resulting from result varying changes in wet and dry season. During the wet season, groundwater level rises towards the surface and drops as the dry season sets in[21].

Figure 1 shows the Geological Map of the Selected Locations of the Study Area within Dahomey Embayment, the inset map showing political divisions of the study area within Nigerian continental environment is shown in Figure 2, the map of the investigated locations in the study area are shown in Figures 3-4 is a base map displaying the location and accessibility of the study area in Ewekoro LGA.

The entire study area is generally accessible by the main roads alongside numerous footpaths, although the road from Abeokuta town to the investigated area is tarred. In addition to Ewekoro-Papalanto road, the survey locations can equally be accessed through a major road from Lagos State through Sango-Ifo express road.

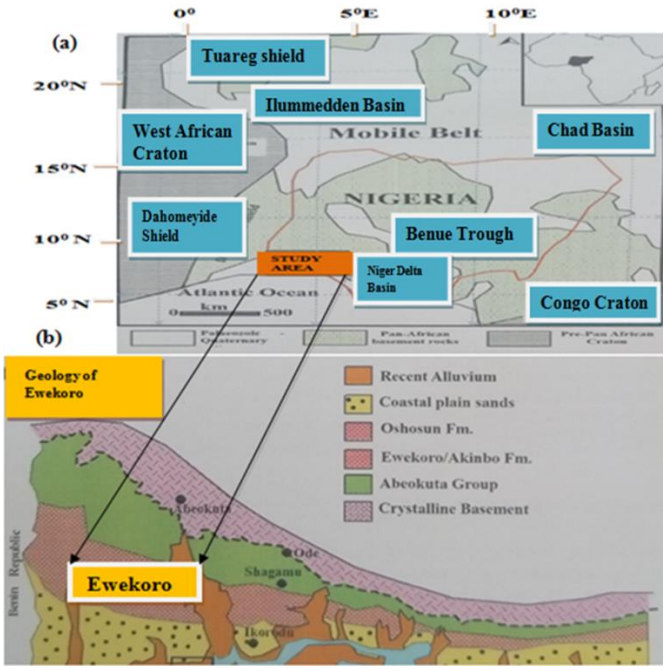

Figure 1. Geological map showing the investigated area within the Nigerian Part of Dahomey Embayment[21 &27]

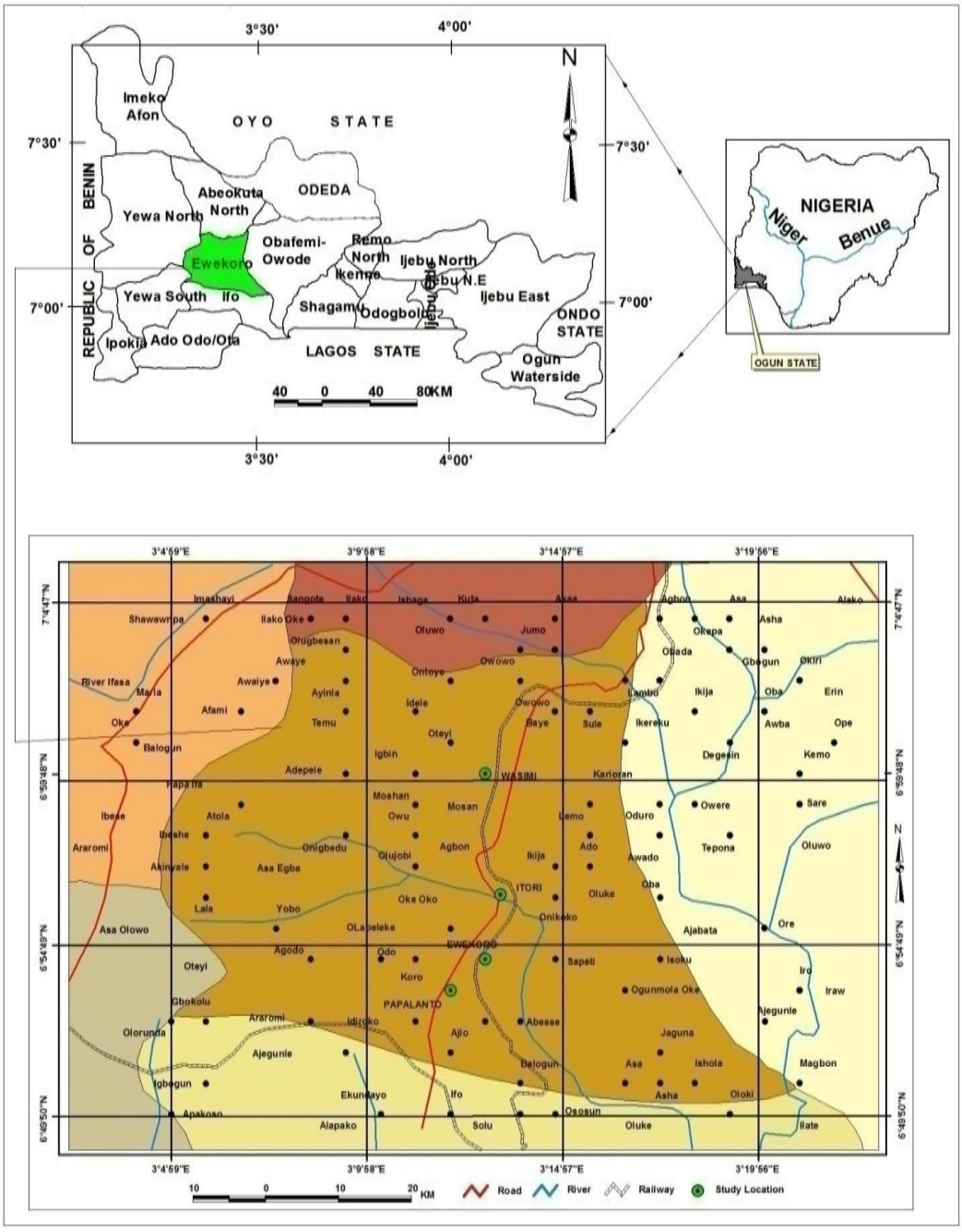

Figure 2. Inset map showing the investigated locations within Nigeria Continental Domain using Esri Data/Nigeria Political Information in Arcview GIS 3.2A Environment[21]

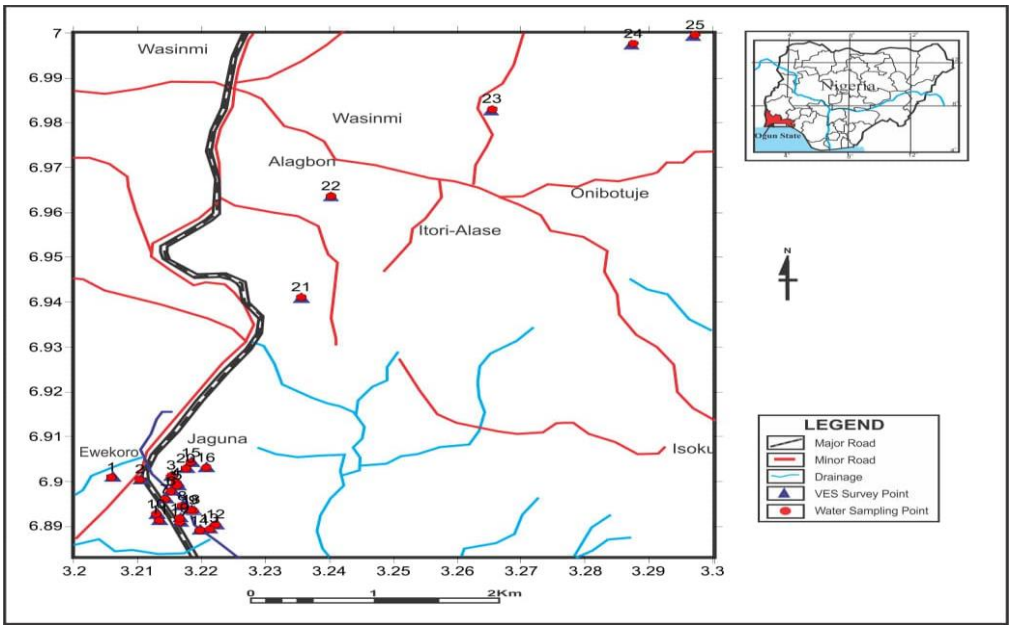

Figure 3. Map showing the data acquisition for the investigated sites in Ewekoro study area, Southwest Nigeria[21]

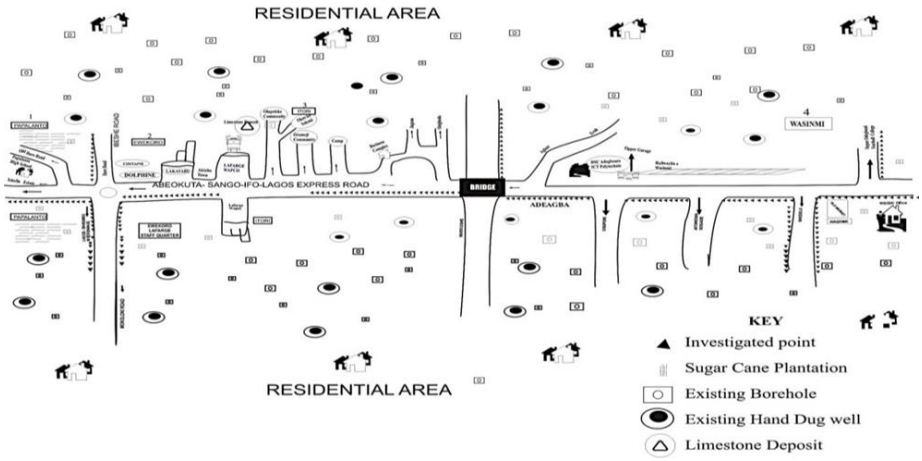

Figure 4. Basemap showing the location and accessibility of the investigated points in Ewekoro LGA, Southwest Nigeria[21]

3. Materials and methods

3.1 Geophysical field data acquisition in Ewekoro

VES and ERT resistivity surveying data were acquired using Integrated Geo and Instrument Services (IGIS), Model: SSR-MP-ATS; Ground Positioning System was used for both coordinate and elevation measurements; Twenty-five vertical electrical soundings and ten 2D electrical resistivity tomography profiles were undertaken respectively for VES and ERT. The work encompassed the utilization of Schlumberger and Wenner electrodes Array. WINRESIST with least square iterative inversion software programs were adopted for 1-D

resistivity inversion; while the RES2DINV.EXE version 3.57.37 iterative software program was adopted for 2-D resistivity inversion; and the contouring of the aquifer parameters was achieved using surfer software program. The vertical electrical sounding investigation adopted Schlumberger electrode array where current was directly sent into the subsurface via a pair of current measuring electrodes denoted as P and Q, and another pair of potential measuring electrodes X and Y responsible for the creation of the resulting potential difference. The apparent resistance R_a of the penetrated subsurface materials was read through the resistivity meter from the crystal displaying the result on the screen. The apparent resistivity was consequently computed by the product of the apparent resistance (R_a) and the geometric factor G, given by the mathematical equations expressed Eq. (1) and Eq. (2):

$$\rho_a = \pi \frac{[(\frac{PQ}{2})^2 - (\frac{XY}{2})^2]}{MN} R_a \quad 1$$

$$G = \pi \frac{[(\frac{PQ}{2})^2 - (\frac{XY}{2})^2]}{XY} \quad 2$$

3.2 Geophysical field data acquisition in Ewekoro

A bilogarithmic graph was used for the plotting of the calculated apparent resistivity, as characterized by a dynamic range for the purpose of smoothening, correcting and overall filtering of outliers that were considered as constituted noise in the field acquired data. This was followed by inverting electronically the already smoothened resistivity curve to true resistivity with the aid of WINRESIST software package. The VES curves were generated by the software program, in turn gave rise to three principal parameters namely true resistivity, thickness and depth. Unit layer resistivities (ρ) as well as the observed depth (h) are the two basic parameters that characterized any given geologic unit and their significance in the background analyses, interpretation and understanding of the given geoelectrical models cannot be overemphasized. These observed parameters served as basic parameters in the derivation of other hydrogeological parameters namely hydraulic conductivity cum hydraulic resistance for the horizontal, homogenous and isotropic layers[23 & 28-29]. The hydraulic conductivity is presented in accordance to the work of Ishola et al. and Heigold et al.[4 & 30] as K in Eq. (3). The hydraulic conductivity of the aquifer protective layers served as a principal parameter in evaluating the level of aquifer vulnerability of the area.

$$K = 386.40 R_W^{-0.93283} \quad 3$$

where K represents the hydraulic conductivity as earlier stated and R_W represents the aquifer resistivity.

The subsurface rocks are porous and well fractured while the hydraulic conductivity gives the description of the ease at which groundwater propagates through the available porous spaces. Aquifer vulnerability index (AVI) has been defined as a technique that evaluates vulnerability considering the hydraulic resistance to vertical propagation of groundwater flow through the overlying strata. The evaluation of AVI utilizes duo parameters namely the thickness (h) of the protective strata and the hydraulic conductivity (k) estimated for the

strata. The hydraulic resistance (C) was consequently calculated by adopting the aforementioned duo parameters and is therefore presented as k_i

$$C = \sum_{i=1}^{n} \frac{h_i}{k_i} \quad [21] \qquad 4$$

Table 1. Aquifer Vulnerability Index (AVI) and Hydraulic Resistance[28]

C	Log C	Vulnerability Status	Vulnerability Code
$0-10$	<1	Extremely High Vulnerability	EHV
$10-100$	$1-2$	High Vulnerability	HV
$100-1000$	$2-3$	Moderate Vulnerability	MV
$1000-10000$	$3-4$	Low Vulnerability	LV
>1000	>4	Extremely Low Vulnerability	ELV

where k_i is repeatedly denoted as hydraulic conductivity, while h_i is represented as the thickness of subsurface materials within the the vadose zone.
Table 1 above illustrates the connecting law between the hydraulic resistance (C) and aquifer vulnerability index (AVI) and serves as aids in evaluating the vulnerability status of any given geologic model. Considering the field 2-D electrical resistivity investigation, the current and potential electrode pairs were increased at 5 m constant spread via the entire measurement until the highest spread is attained. The implication is that the series of measurement were observed in consecutive steps of 5 m, 10 m, 15 m, 20 m, and so on, progressively till the exhausted highest spread length of 200 m was reached. The conversion of the apparent resistivity was done using measured resistance at different intervals through the expression given in equation 5:

$$\rho_a = 2\pi a\, R_a \qquad 5$$

where the electrode spread is denoted by a and the resulting resistivity values were utilized in the generation of the ERT model utilizing the RES2DINV.EXE software program.

4. Results

4.1 Output of the VES data

The computer iteration of the resistivity soundings displayed in Figure 7 reveals the curves representing the inverse model of the geoelectrical parameters while the observed geoelectrical parameters as derived from the inverse model curves are hereby displayed in Table 1. On a general note, the resistivity sounding curves obtained from the surveyed area was a typical 4 layer (H type), with few 5-layer (KH). The H-type curve with about 85.4% of occurrence and KH-type curve with about 14.6% of occurrence were deduced from the area. Worthington et al. revealed that the curves as obtained from the field often reflect image geoelectrically revealing the condition of the area lithologic units in sequence and as a result this can be can be qualitatively utilized in assessing the groundwater prospects of

the area[31]. The H and KH curves are typical curves often serve as reflections of probable groundwater occurrence are pertinent to the study area[32]. The geoelectrical parameters of the lithologic units from the interpreted sounding curves were delineated as shown on Table 2 since electrical resistivity methods are basic reflection of the observed changes in earth resistivity[4 & 33-35]. Considering the consistency of the geoelectrical parameters, the layers delineated in the midst of the sounding curves were specifically shown particularly along deeper sections of relatively uniform model resistivities and thicknesses (Table 2). The establishment of the lithology for the delineated geoelectrical layers was achieved by the integration the available information acquired from the previous drilled-well core samples as obtained from boreholes and hand-dug wells, observed local geology and previous published studies[36-41]. The geoelectrical layers that were then delineated ranking from top to bottom were typified as top soil, sandy clay/clayey sand, shale/clay, sand lens, lateritic/kaolinitic clay, clayey sand, clay/shale, sandstone, weathered limestone and saturated sandstone. The topsoil is primarily of lateritic soil and partly unconsolidated sandy clay constituents with observed resistivity value that ranged from 26.90 to 842.20 Ωm with a mean value of 177.96±250.28. Lateral continuity was observed across the study area of resistive layer underlain the top soil; characterized as sandy clay/clay/clayey sand. The large observed variation in the model resistivity of this layer is a resultant effect of the differences in the extent of compaction of the unit alongside the lateral variations in constituent minerals. The second geoelectrical layer is underlain by sandy clay or shale/clay unit that is laterally discontinuous and characterized by a low resistivity while the lithological units were karstic limestone, saturated sandstone and sand. The delineated aquiferous layers were overlain by these top layers. Compaction and lithification were the possible attributes that accounted for the high resistivity values as observed in these layers. Large variations were observed in confined differentiation status of aquifer types. The borehole locations associated with VESEWE7 and VESEWE8 alongside with VESEWE14, VESEWE15, VESEWE21, VESEWE24 and VESEWE25 boreholes are unconfined while the rest locations displayed confined aquiferous conditions (Table 2).

4.2 Groundwater vulnerability in terms of aquifer protective capacity

In hydrogeological field studies, aquifer transmissivity is expressed to be resultant multiplication of its hydraulic conductivity for the thickness of the layer while the resultant multiplication of the resistivity for its thickness is defined and consequently represented as being the transverse unit resistance (T_r), on a pure theoretical basis. Therefore, the transmissivity of any aquiferous unit gave a direct proportionate increase to its transverse unit resistance directly and vice-versa[42]. Low resistivities and low hydraulic conductivities are typical of clay dominated layers. Hence, the protective capacity of the overburden unit could be regarded as being proportional to the ratio of the thickness to resistivity of the unit. In all the investigated study locations displayed less 1.0 protective capacity values except VESEWE9 and VESEWE17 whose protective capacities are greater than 1.0 Siemens with VESEWE17 being the investigated location with the highest protective capacity. The values range from 7.7002×10^{-3} Siemens to 1169.48×10^{-3} Siemens (Table 1).

Table 2. Computed geoelectrical parameters of Ewekoro

VES Stations	Aquifer Resistivity $\rho_a(\Omega m)$	Depth to Aquifer (m)	Longitudinal Conductance (S)	Probable Aquifer System	Inferred Lithology	Hydraulic Conductivity (m/s)	Transmissivity (m^2s)	Protective Capacity ($Siemens$)
VESEWE1	26.7	46.9	**0.5801**	Confined	Limestone/Sandstone	44.39085×10^{-3}	1025.4287×10^{-3}	865.31×10^{-3}
VESEWE2	281	**8.04**	0.1041	Confined	Limestone/Sandstone	7.114064×10^{-3}	227.65000×10^{-3}	387.935×10^{-3}
VESEWE3	104	37.7	0.2351	Confined	Limestone/Sandstone	25.44385×10^{-3}	694.61675×10^{-3}	659.607×10^{-3}
VESEWE4	175	74.1	0.2653	Confined	Limestone/Sandstone	15.26058×10^{-3}	1066.7150×10^{-3}	833.333×10^{-3}
VESEWE5	**7.55**	32.6	**0.5290**	Confined	Limestone	50.95356×10^{-3}	1650.8934×10^{-3}	529.049×10^{-3}
VESEWE6	419	39	0.0824	Confined	Limestone	2.633922×10^{-3}	81.651544×10^{-3}	721.293×10^{-3}
VESEWE7	74.06	65.76	0.3538	Unconfined	Limestone	31.56477×10^{-3}	1952.2807×10^{-3}	701.158×10^{-3}
VESEWE8	96.3	70	0.3195	Unconfined	Limestone	26.89435×10^{-3}	1758.8856×10^{-3}	682.934×10^{-3}
VESEWE9	88.2	83	0.5131	Confined	Limestone/Sandstone	28.50939×10^{-3}	481.80866×10^{-3}	$\mathbf{1128.33\times10^{-3}}$
VESEWE10	70.3	57.9	0.3901	Confined	Limestone/Sandstone	32.43096×10^{-3}	716.72424×10^{-3}	740.079×10^{-3}
VESEWE11	166	9.83	0.0377	unconfined	Limestone	16.28222×10^{-3}	491.72292×10^{-3}	100.807×10^{-3}
VESEWE12	366	11.9	0.0247	unconfined	Limestone	3.857709×10^{-3}	108.40162×10^{-3}	100.671×10^{-3}
VESEWE13	615	13.35	0.0136	unconfined	Limestone	$\mathbf{0.642283\times10^{-3}}$	$\mathbf{3.5967838\times10^{-3}}$	143.962×10^{-3}
VESEWE14	**4765**	11.8	**0.0082**	Unconfined	Limestone	6.776527×10^{-3}	1910.9807×10^{-3}	323.312×10^{-3}
VESEWE15	126	15.13	0.0498	Unconfined	Limestone	21.71652×10^{-3}	275.79986×10^{-3}	94.9367×10^{-3}
VESEWE16	99.2	61.2	0.3629	Confined	Limestone/Sandstone	26.33855×10^{-3}	758.55612×10^{-3}	885.341×10^{-3}
VESEWE17	1.03	61.2	1.1468	Confined	Limestone/Sandstone	53.40249×10^{-3}	1537.9919×10^{-3}	$\mathbf{1169.48\times10^{-3}}$
VESEWE18	175	**96.6**	0.3453	Confined	Limestone+Sand	15.26059×10^{-3}	1429.9170×10^{-3}	1122.81×10^{-3}
VESEWE19	123	56.1	0.2879	Confined	Limestone	22.19070×10^{-3}	532.57690×10^{-3}	782.779×10^{-3}
VESEWE20	106	62.5	0.3427	Confined	Limestone	25.08007×10^{-3}	438.90121×10^{-3}	809.561×10^{-3}
VESEWE21	163	71	0.0012	unconfined	Limestone+Sand	16.63774×10^{-3}	953.34237×10^{-3}	9.88459×10^{-3}
VESEWE22	407.2	54	0.0026	Confined	Limestone+Sand	2.867480×10^{-3}	139.64626×10^{-3}	61.6017×10^{-3}
VESEWE23	438.5	60.3	**0.0007**	Confined	Limestone+Sand	2.288905×10^{-3}	108.49409×10^{-3}	24.4968×10^{-3}
VESEWE24	139.4	37.4	0.0021	Unconfined	Limestone	$\mathbf{197.1921\times10^{-3}}$	$\mathbf{5639.6951\times10^{-3}}$	$\mathbf{7.70015\times10^{-3}}$
VESEWE25	80.8	74	0.0296	Unconfined	Limestone	37.86069×10^{-3}	1847.6019×10^{-3}	36.2018×10^{-3}

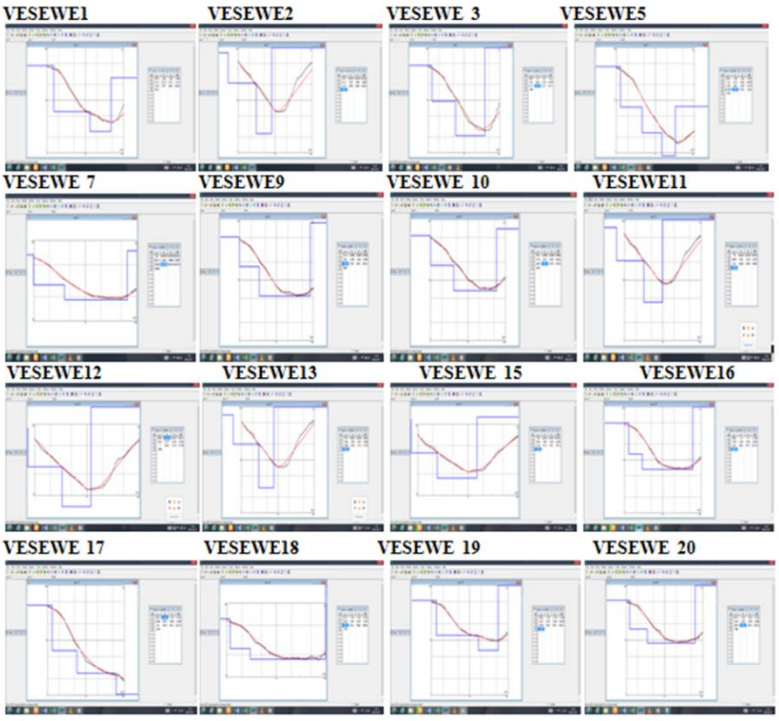

Figure 5. Typical VES curves representing investigated sounding points in Ewekoro[21]

In the entire study locations where the longitudinal conductance (*S*) and hence, the protective capacity (P_c) values in the study areas are less than 1.0 Siemens (P_c < 1.0 Siemens); they are classified as low and are characteristics of depositional successions of overburden layers with no impermeable clay/shale appreciably overlying rock. Such subsurface model is suggestive of high rates of infiltration from precipitation as well as surface contaminants into the aquifer system. However, the investigated locations where the protective capacity values are greater than 1.0; P_c < 1.0 Siemens (VESEWE9 and VESEWE17); imply that these locations have considerable layers of Clay separating the subsurface aquiferous zones (Table 1). In addition to high transmissivity and low protective capacity values in most of the investigated sites in the study area, the aquifers were very close or relatively close to the surface (<100m) and thus prone or susceptible to contamination over large areas once the aquifer receives a load of contaminant dose from surface to near surface. Nevertheless, groundwater potential in this study area is high due to high transverse unit resistance (*R*) with good suitability for the development of potable water supply boreholes [21].

4.3 Aquifer vulnerability potentials using 2D electrical resistivity imaging

The inversion of the observed apparent resistivity pseudosection and inverse model resistivity section gives the 2D model resistivity of the subsurface. The figures were generated through the use of robust software called RES2DINV. Consequent to the resultant output of the subsurface geological situations of the investigated area being typically sedimentary, the resistivity values show the structure of the study areas in layers. A trend of the general geoelectrical-lithology of the subsurface somewhat related to result observed in resistivity as typically revealed in the inverse models of the 2D resistivity. Existence of reasonable correlation is observed between the 2D inverse models and the delineated geoelectrical layered parameters derived from the sounding curves. Also, the lateral continuities of geoelectrical layer (geoelectrical-lithology) and near-surface heterogeneity observed in the resistivity soundings were depicted conspicuously in the inverted 2D resistivity images. It is worthy of note that the delineated topsoil observed in the resistivity soundings (VES) was not distinct in the 2D images (2D-ERT); this is as a result of its very small thickness values that ranged from 0.4m to 1.7m averaging 1.11m in relation to the minimum electrode spread of 10.0m adopted for the 2D survey in the study area (Figures 6 through 10).

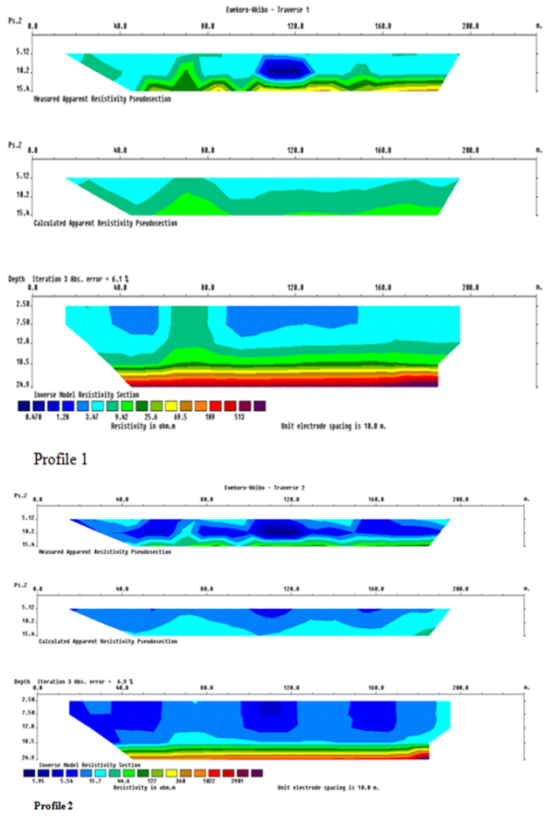

Figure 6. 2D-ERT inverse model along Ewekoro tranverse 1 (Profiles 1 and 2)

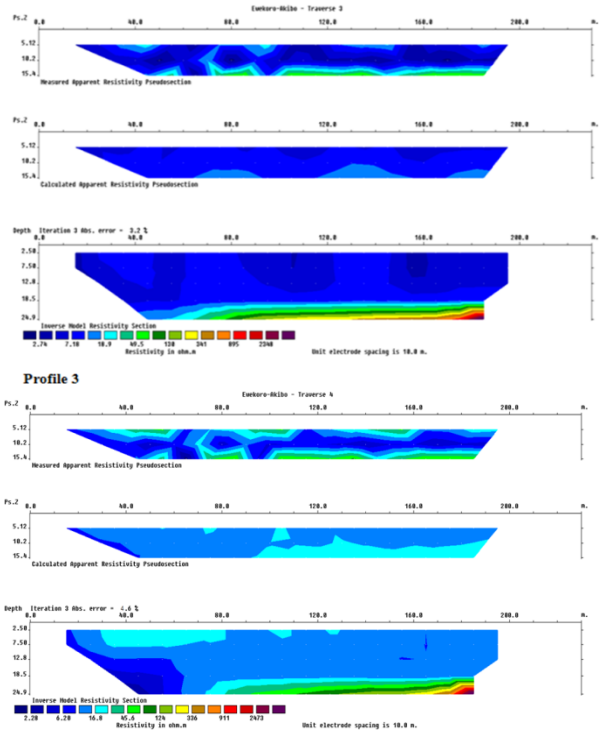

Figure 7. 2D ERT inverse model along Ewekoro tranverse 2 (Profiles 3 and 4)

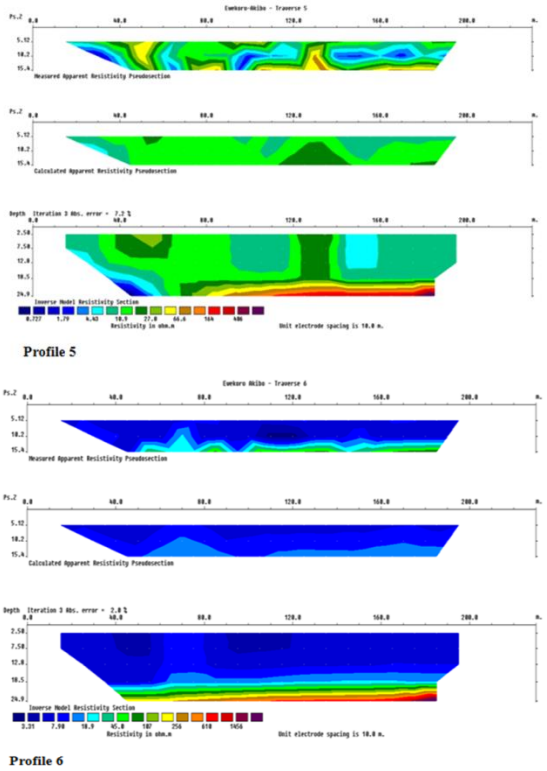

Figure 8. 2D ERT inverse model along Ewekoro tranverse 2 (Profiles 5 and 6)

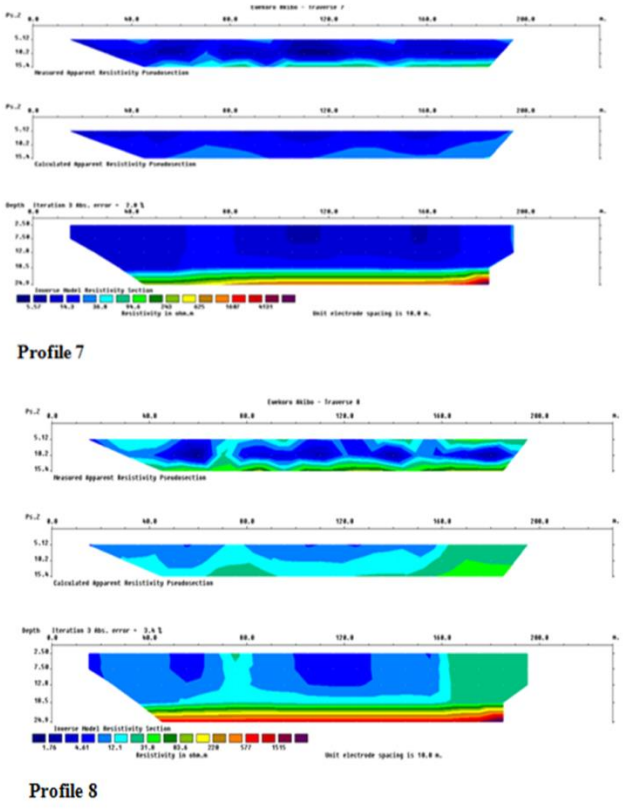

Figure 9. 2D ERT inverse model along Ewekoro tranverse 2 (Profiles 7 and 8)

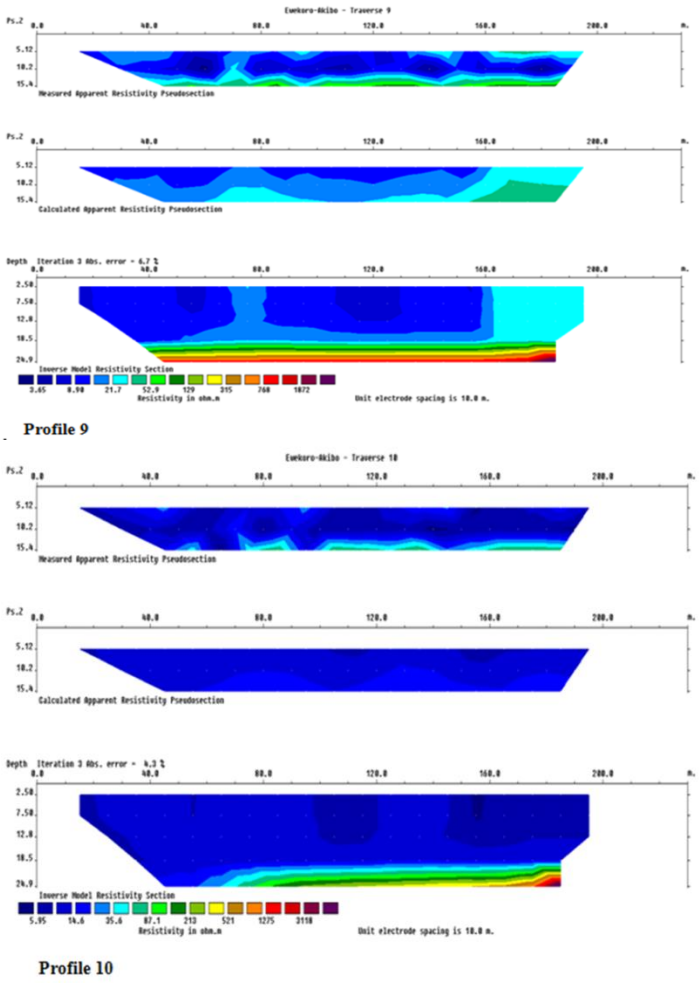

Figure 10. 2D ERT inverse model along Ewekoro tranverse 2 (Profiles 9 and 10)

5. Discussion

5.1 Geoelectric interpretation of subsurface lithology in Ewekoro

5.1.1 Tranverse 1 (Profiles 1and 2)

Profile 1 inverse resistivity model (Figure 6) revealed very low resistivity anomalies below 3.47Ωm at lateral positions between 35m to 58m and 90m to 150m from the surface of the section to depths of about 10m. Highly conductive zones were noticed from the surface to depths of about 17m at lateral distances of approximately 15m to 65m and 80m to 200m. The conductive zone is inferred to be typically Clay underlain by Clayey sand with different degree of saturation. Bedrocks with higher resistivity values above 513 Ωm constitute the base of the section.

Profile 2 inverse resistivity model equally revealed very low resistivity anomaly at horizontal distances between 15m to 59m, 96m to 123m and 148m to 170m as three principal condensed regions of very high conductivity with resistivity values below 1.95 Ωm from the surface of the section to depths of 20m, 15m and 15m respectively. These

areas indicate possible leachate accumulations in the Clayey sand bed which displayed a wide and continuous spread of low resistivity zones which laterally extends from 15m to 200m. The relatively high resistivity values encountered can be attributed to different degrees of mineralogical composition of the solid rock at the base of the section underlying the Clay layers (Figure 6).

5.1.2 Tranverse 2 (Profiles 3 and 4)

Profile 3 inverse resistivity model (Figure 7) showed three conductive zones with very low electrical resistivity signature below 2.74 Ωm at approximated lateral distances of about 15m to 25m, 48m to 51m 83m to 122m and 146m to 200m at depth not greater than 20m. This region dominates the leachate accumulation and migration. This region was suggested to be Clay soil with varying degree of saturation and possible migration of contaminant seepages to the underlying rock materials.
Profile 3 inverse resistivity model possess resistivity values that ranged from 2.28Ωm to 2473 Ωm. The possible contaminant plumes could only be found at the NW edge of which migrated laterally and vertically downwards from the surface continuously until it merges with the depth of 24.9m as it stretches gradually from the lateral position of 15m to 64m. This suggested that the massive contaminant plume migration into the subsurface might have possibly reached the water table thereby polluting the regional groundwater system (Figure 7).

5.1.3 Tranverse 3 (Profiles 5 and 6)

Profile 5 inverse resistivity model (Figure 8) revealed resistivity values that ranged from 0.73 Ωm to 406 Ωm. The confined blue portion shows the possible leachate conductive zones with resistivity values below 0.73 Ωm which accumulated at the bottom of the section at lateral position of 38m to 54m; this suggested that the contaminant plumes must have percolated slowly down to the subsurface due to the predominance of Clayey sand and presence of rocks that have been fractured/weathered found dominating the model with resistivity values ranging from 10.9 Ωm- 27.0 Ωm while the bedrock displayed resistivity values of about 406 Ωm.
Profile 6 inverse resistivity model showed two regions of possible contaminant accumulations with resistivity values below 3.31Ωm from the surface of the model to a depth of about 10m at lateral positions of about 39m to 55m and 90m to 120m. Enclosing the conductive regions were materials suspected to be Shale/Clay materials mixed with decomposing wastes which covers about 80% of the entire section with considerable and relatively consistent thickness. The migrations of contaminant seepages from the surface to the condensed region were well observed from the surface of the section to depths of about 20m. This was due to the fairly steep topography of the site. Clayey sand probably mixed with water and weathered rock materials were observed laterally beneath the conductive zones at lateral distance of about 35m to 200m with the observed resistivity that ranged in values from 18.9 Ωm to 107 Ωm (Figure 8).

5.1.4 Tranverse 4 (Profiles 7 and 8)

Profile 7 inverse resistivity model (Figure 9) showed three possible regions of high conductivity with resistivity value below 5.57 Ωm from the surface of the section to depths of about 13m to 20m at lateral profile length of about 15m to 162m and 81m to 173m respectively. These regions cover about 80% of the entire section with considerable thickness of lateral and vertical migrations across the entire section. The massive and extensive nature of these regions across the section inferred to be Sandy clay suggested possible leachate accumulations and migration which could have impeded the subsurface with consequent lethal impacts on the local and regional groundwater system of the area. Underlying these regions is Clayey sand which is in turn laterally underlain by weathered rock materials and bedrocks of much higher resistivity values that range from 243 Ωm-4131 Ωm observed only at the base of the section.

Profile 8 inverse resistivity model showed very low resistivity anomalies below 1.76 Ωm of lateral extension of approximate distance of 15m to 20m, 38m to 43m and 98m to 131m from the surface of the section to a consistent depth of about 10m depicting regions of condensed zone of very high conductivity. Generally, conductive zones were observed from the surface to depths of about 20m at lateral distances of about 15m to 162m enclosing the condensed region of possible accumulations and migrations of contaminant seepages. Sandy clay enclosed these conductive zones and in turn underlain by Clayey sand while a uniform, continuous and lateral distribution of weathered rock materials and bedrocks of much higher resistivity values ranging from 31.8Ωm to 1515 Ωm were found at the lower section (Figure 9).

5.1.5 Tranverse 5 (Profiles 9 and 10)

Profile 9 inverse resistivity model (Figure 10) showed near surface low resistivity values below 3.63 Ωm from the surface of the section to depths of about 20m and 19m at lateral extension of about 15m to 70m and 82m to 159m respectively. These low resistivity zones which indicated the presence of Sandy clay mixed with decomposing wastes cover the middle of the model and were more condensed at the NW and centralized area of the section compared to the extremes of the SE. Underlying the conductive zone are Clayey sand formation and weathered rock materials probably containing Clay sand were noticed beneath this zone extending uniformly and continuously at considerable lateral distance of 38m to 200m.

Profile 10 inverse resistivity model revealed a similar near surface low resistivity values below 5.95 Ωm from the surface of the section to depths of about 3m. Three condensed region of very high conductive zones were delineated and enclosed by a Sandy clay formation which spreads widely, uniformly and continuously at a lateral extension of 15m to 200m. It is thicker in the NW than in the middle and SE section of the model. These enclosed conductive zones are underlain by Clayey sand materials which are underlain in turn by Limestone and the basal Sandstone formation of varying higher resistivity values ranging from 521Ωm - 3118 Ωm (Figure 10).

5.2 Vadose zone characterization of geohydraulic parameters in Ewekoro

The two geohydraulic parameters specifically termed as hydraulic conductivity and hydraulic resistance were computed utilizing the integration of the principal geoelectrical

parameters namely the resistivity and depth of the layers above the aquiferous zone by adopting earlier stated equations; equation 3 and equation 4 respectively (Table 3). The observed hydraulic conductivity (k) ranged from 0.0082 cm/s in VESEWE24 to 5.149cm/s in VESEWE1 while the corresponding hydraulic resistance (C) which evaluates groundwater vulnerability extent ranged from 0.0075 day^{-1} in VESEWE21 to 15,445.98 day^{-1} in VESEWE25. The observed variation of these parameters is an indication of the argillaceous materials presence in the subsurface sediments and this typically characterizes the dynamic behavior of an aquifer to allowing groundwater flow through their protective layers. Very low to moderate and very high resistivity values from 1.0 Ωm to 4765 Ωm were identified. VESEWE1, VESEWE5, VESEWE8 VESEWE9, VESEWE10, VESEWE16 VESEWE17 and VESEWE25 possessing relatively much higher groundwater potentials values judging by the observed layer resistivity falling below 100 Ωm[4].

Table 3. Vadose zone estimation of geohydraulic parameters in Ewekoro

Lithology	Latitude (°E)	Longitude (°N)	Thickness (m)	Aquifer Resistivity ρ_a(Ωm)	K(cm/s)	C(day)	Log C	Vulnerability Implication
VESEWE1	3.202968	6.901082	46.9	26.7	5.1484534	1.0462	0.0196	EHV
VESEWE2	3.202409	6.900684	**8.04**	281	4.6217266	0.1911	- 0.7187	EHV
VESEWE3	3.201068	6.900384	37.7	104	5.020695	0.8390	- 0.0762	EHV
VESEWE4	3.200722	6.901373	74.1	175	4.4872873	1.7922	0.2534	EHV
VESEWE5	3.203448	6.899762	32.6	**7.55**	5.1004887	0.7500	- 0.1249	EHV
VESEWE6	3.203242	6.899873	39	419	5.09535	0.8619	- 0.0646	EHV
VESEWE7	3.201905	6.899289	65.76	74.06	4.3936151	1.6296	0.2121	EHV
VESEWE8	3.201783	6.897345	70	96.3	4.29138	1.7602	0.2456	EHV
VESEWE9	3.202085	6.900732	83	88.2	4.7876915	1.8734	0.2726	EHV
VESEWE10	3.203467	6.884735	57.9	70.3	4.7430878	1.3395	0.1269	EHV
VESEWE11	3.200053	6.894753	9.83	166	4.6283867	0.4542	- 0.3428	EHV
VESEWE12	3.199405	6.893631	11.9	366	4.4840577	0.2893	- 0.5386	EHV
VESEWE13	3.198532	6.885386	13.35	615	4.6651891	0.1846	- 0.7337	EHV
VESEWE14	3.198926	6.892652	11.8	**4765**	4.6685492	0.2789	- 0.5546	EHV
VESEWE15	3.200106	6.885736	15.13	126	4.0482649	0.3888	- 0.4103	EHV
VESEWE16	3.191532	6.890598	61.2	99.2	4.9063406	1.3937	0.1442	EHV
VESEWE17	3.201839	6.893456	61.2	1.03	0.5135496	2.2704	0.3561	EHV
VESEWE18	3.196568	6.894773	**96.6**	175	4.5164594	2.3716	0.3751	EHV
VESEWE19	3.193248	6.942893	56.1	123	4.9275818	0.1348	- 0.8702	EHV
VESEWE20	3.199006	6.943245	62.5	106	4.7980441	1.4339	0.1565	EHV
VESEWE21	3.197998	6.942646	71	163	1.545965	**0.0075**	- **2.1238**	**EHV**
VESEWE22	3.199175	6.891007	54	407.2	1.3319025	4.1530	0.6184	EHV
VESEWE23	3.199152	6.893687	60.3	438.5	0.1433435	60.6241	1.7827	HV
VESEWE24	3.194219	6.892001	37.4	139.4	0.00814565	61.6705	1.7901	HV
VESEWE25	3.197942	6.903056	74	80.8	1.7409803	15445.98	4.1888	ELV

5.3 Variation of hydraulic parameters of Ewekoro aquifer and its vulnerability implication

The variation of the aquifer parameters at different locations in the study area are displayed in Figures 11, 12 and 13 respectively contoured for aquifer resistivity map, overburden thickness map and hydrulic conductivity map. This variation is evidently seen in the fairly steeply dipping slopes in the larger portion of the map. In the 3D map representation (Figure 13) there is only one visible and prominent peak which correspond to the area with the highest resistivity value (VESEWE14) in 2D.

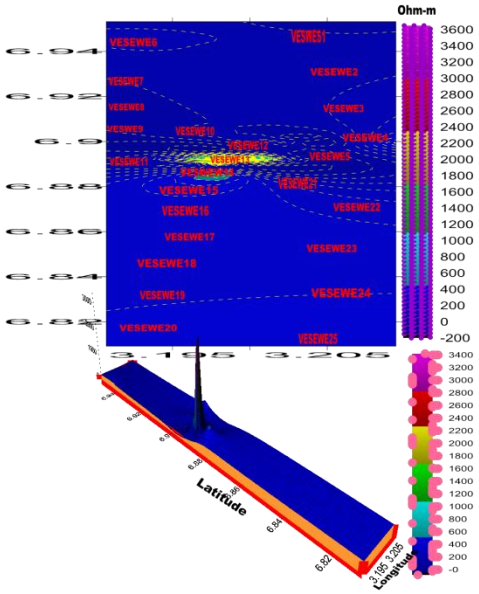

Figure 11. 2D/3D -view of the aquifer resistivity map of Ewekoro

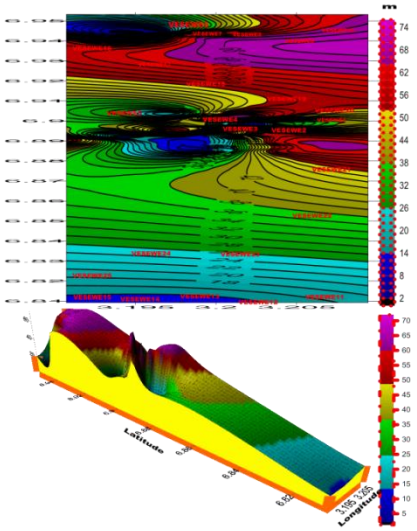

Figure 12. 2D/3D -view of the overburden thickness map of Ewekoro

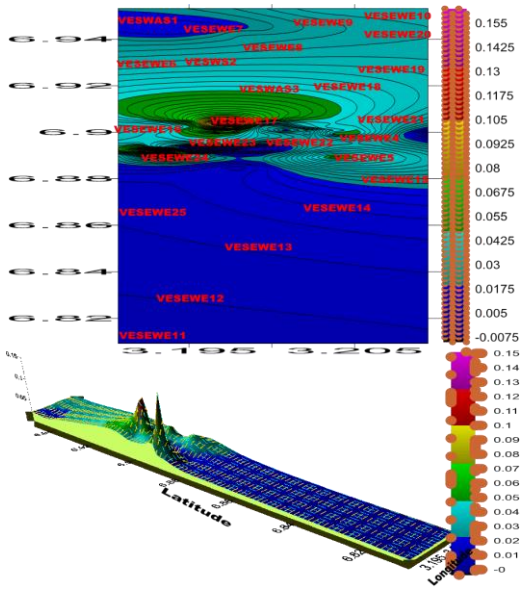

Figure 13. 2D/3D – view of the hydraulic conductivity map of Ewekoro

The resistivity values appearing most frequently ranged between 41 ohm-m and 58 ohm-m suggestive of materials of slight clayey and/or saturated with water[43]; typically made of saturated clay but poorly permeable to the interstitial formation for the abstraction of groundwater[44]. The depth to overburden is greatest at VESEWE9 with a very high overburden thickness value of 83m found at the North-East section of the map with a conspicuous rise. VESEWE4 (74.1m), VESEWE10 (57.9m), VESEWE16 (61.2m), VESEWE17 (61.2m), VESEWE19 (56.1m), VESEWE20 (62.5m), and VESEWE22 (53.9m) depicted considerably very high overburden thickness values. High overburden thickness is equally observed in some other VES locations the study area; these are VESEWE1, VESEWE3, VESEWE5 and VESEWE6, while the area possessing the thinnest overburden is found in VESEWE18 (2.97m) seen at the Southwest section of the map 2D (Figure 12). Areas with VES stations whose overburden thickness values were higher than 26.0m were consequently regarded to be of better groundwater potentials compared to other locations possessing lower overburden thickness values. In this area, larger portion of the locations in the North-East section of the map have their overburden thickness greater than 26m while some sizeable portions of the locations in the South-West of the map have their overburden thickness less than 26m; these are VESEWE2, VESEWE7, VESEWE8, VESEWE11, VESEWE12, VESEWE13, VESEWE14, VESEWE15, VESEWE18, VESEWE21, VESEWE23 and VESEWE24 while locations with overburden thickness values between 1m and 10m above are hereby considered as low/thin overburden thickness. The overburden thickness values of limestone aquifer contoured in this section (Figure 12) clearly depicted the varying depths of the encountered limestone in all the investigated profiles. As the overburden thickness consisting all materials overlying the basal limestone strata, it reveals aquifers occuring at various depths across the investigated locations[45-46]. The generated contour-map reveals a section of thick overburden/depression, displayed by the observed dense contour closures across different sections of the investigated locations. Regions of varying thin overburden/depression are however also observed along other parts. The areas with high overburden thickness when compared with the resistvity values showed very low aquifer resistivity values which discloses the existence of saturation zones

beneath the limestone strata while the the overburden serve as a protective coverage shielding the targeted groundwater reservoir from possible pollution migrating from the surface. Furthermore, variation in hydraulic conductivity is also observed in most investigated sites in the study area except VESEWE24 with the highest hydraulic value of 197.1921×10^{-3} m/s with prominent peak having a small area of spread as shown in the 3D map in association with few other locations with fairly high hydraulic conductivity values; VESEWE5, VESEWE17 and VESEWE25 while VESWEWE14 has the lowest hydraulic conductivity value of 6.776527×10^{-17}m/s (Figure 13). Hydraulic resistance serves as an indispensable geoelectrical formation parameter often utilized in estimating the extent of the resistance of an aquifer to fluid flow vertically via the protective overlying layers while the connection between the aquifer vulnerability index (AVI), C and log C displayed in Table 3 reveals that AVI in most of the investigated sites were extremely high (88%) in accordance to the adopted grading of Stempvoort et al.[28], as VESEWE23 and VESEWE24 (8%) exhibited high vulnerability status and only VESEWE25 depicted low vulnerability status (4%). The ERT profiles (Figures 6-10) reveal the vertical and lateral changes in resistivity along the subsurface in area. Generally, we can infer from the resistivity changes that the percolation of contaminant seepages (leachates) is not only surficial in some investigated but has invaded aquifers in other locations judging by the depth to the aquifer as seen in Table 2, indicating that the aquiferous zones of the study area are generally vulnerable or prone to contaminant seepages. The location around VESWAS25 with extremely low vulnerability may consequently be the resultant effect of the compact nature of the investigated locations (Table 3).

6. Conclusions

The VES and ERT outputs were utilized in evaluating the aquifer vulnerability status of the investigated area. The application of the resistivity techniques of geophysical prospecting enabled the extrapolation of geoelectrical and consequent hydraulic parameters. The changes in the recorded geoelectrical parameters depicted low to relatively high resistivity values across the investigated area. The (ERT) is in agreement with the observed VES sounding results where high resistivity values were observed at the aquifer layer. The basic properties comprising of resistivity and thickness of the protective strata were utilized in the estimation of hydraulic conductivity cum hydraulic resistance required for the evaluation of the aquifer vulnerability index (AVI) for the later classification of the vadose zone vulnerability implications. The ERT profiles revealed the vertical and lateral heterogeneities of the subsurface, and the output of the profiles were reflections of low to relatively high resistivities across the subsurface both at lateral and vertical extents. The computed geohydraulic parameters provided the necessary geoelectrical details considering the aquifer protective strata which enhanced the identification and consequent description of the vulnerability status of the delineated aquifer layers. The observed notable changes of the computed aquifer parameters as revealed in the generated contour maps both in 2D and 3D representations are reflections of consequent changes in the subsurface hydrogeological formations that are relatively inhomogeneous. The integration of AVI and ERT alongside VES investigations in this investigation gave a comprehensive outcome of the groundwater protection status of the investigated area revealing the extent of protection in the entire

locations within the study area in relation to their susceptibility to contaminant seepages. These parameters hereby provided the required information necessary for groundwater resource management studies and equally serve as control measures to assessing the vulnerability conditions of saturation zones in consequent to the subsurface geology of the study area.

7. References

1. Hinsby, K; Purtschert R & Edmunds, M. 2006. Groundwater age and water quality vulnerability. In: Quevauviller P (Ed) Groundwater Science and Policy. *Chemical Society Reviews, CSR* (In Prep): 6-10.
2. George JN; Ibuot JC & Obiora DN. 2015a.Geoelectrohydraulic of Shallow sandy in Itu, Akwa-Ibom State (Nigeria) using geoelectrical and hydrogeological measurements. *Journal of African Earth Sciences*, 110 (2): 52–63.
3. Obiora DN; Ajala AE & Ibuot JC. 2015. Evaluation of aquifer protective capacity of overburden units and soil corrosivity in Makurdi, Benue State, Nigeria using electrical resistivity method. *Journal of Earth System and Science*, 124 (1): 125–135.
4. Ishola, SA; Makinde, V; Aina, JO; Ayedun, H; Akinboro, FG; Okeyode, IC; Coker JO & Alatise, OO. 2016. Aquifer protection studies and groundwater vulnerability assessment in Abeokuta South Local Government Area, South-West Nigeria, *Journal of Nigerian Association of Mathematical Physics*, 33 (1): 347-362.
5. Ishola, SA. 2024a. Groundwater protection assessment using frequency domain electromagnetic method and direct current electrical resistivity method in Papalanto South-West Nigeria.Nigerian *Journal of Theoretical and Environmental Physics*, 2 (1): 1-27. https://doi.org/10.62292/njtep.v2i1.2024.1.
6. Ishola SA. 2024b. Aquifer characteristics and groundwater reservoir protective capacity rating in Obafemi-Owode Local Government Area, Ogun State South-West Nigeria. *Federal University Wukari (FUW) Trends in Science and Technology Journal*, 9 (1): 392-398. www.ftstjournal.com.
7. Bjerg, PL; Hinsby K; Christensen, TH & Gravesen, P. 1992. Spatial variability of hydraulic conductivity of an unconfined sandy aquifer determined by a mini slug test. *Journal of Hydrology*, 136 (1-4): 107–122.
8. Hossain ML; Das SR & Hossain, MK. 2014. Impact of landfill leachate on surface and groundwater quality.*Journal of Environ Science and Technology*, 7 (1): 337-346.
9. Ibuot, JC; Obiora, DN; Ekpa, MM & Okoroh, DO. 2017. Geoelectrohydraulic Investigation of the surficial aquifer units and corrosivity in parts of Uyo L. G. A., Akwa-Ibom, Southern Nigeria. *Journal of Applied Water Sciences*, 7 (1): 4705-4713.
10. Ugwuanyi, MC; Ibuot, JC & Obiora, DN. 2015. Hydrogeophysical study of aquifer characteristics in some parts of Nsukka and Igbo Eze South Local Government Areas of Enugu State, Nigeria. *International Journal of Physical Sciences*. 10 (15): 425-435.
11. Hölting, B; Härtlé, T; Hohberger, KH; Nachtigall, KH; Villinger, E; Weinzierl, W; Wrobel, JP 1995. KonzeptzurErmittlung der Schutz- funktion der Grundwasserüber- deckung.*Geol Jb* , 63 (1): 5-24.
12. Weatherington-Rice, J; Christy, SD; Angle, MP; Gehring, R & Aller L. 2006. Drastic hydrogeologic settings modified for fractured tills: Part 1 Theory and Part 2 Field Observations. *Ohio Journal of Science*, 106 (2): 45-63.
13. Stempvoort, D; Ewert, L & Wassenaar, L. 1992. AVI: A method for groundwater protection mapping in the prairie Provinces of Canada. *Prairie Provinces Water Board Report*, 1 (14): 13-14.
14. Samsudin, AR; Rahim, B; Yaacob, WZW & Hamzah U. 2009. Mapping *of Contamination Plumes at Municipal Solid Waste Disposal Site Using Geotechnical Imaging Technique*, A Case Study in Malaysia. *Journal of Spatial Hydrology*, 6 (2): 13-22.

15. George, NJ; Emah, JB & Ekong, UN. 2015b. Geohydrodynamic Properties of Hydrogeological Units in Parts of Niger Delta, Southern Nigeria. *Journal of African Earth Sciences,* 105 (2): 55–63.
16. Obiora, DN; Ibuot, JC & George, NJ. 2016. Evaluation of aquifer potential, geoelectrical and hydraulic parameters in Ezza North, Southeastern Nigeria, using geoelectrical sounding. *International Journal of Environmental Science Technology,* 13 (2): 435-444.
17. Lashkaripour, GR & Nakhaei, M. 2005. Geoelectrical investigation for the assessment of groundwater conditions; a Case Study.*Ann Geophys*, 48 (6): 937-944.
18. Ibuot, JC; Akpabio, GT & George, J. 2013. A survey of the repositories of groundwater potential and distribution using geoelectrical resistivity method in Itu Local Government Area (LGA), AkwaIbom State, Southern Nigeria. *Cent Eur J Geosci*, 5 (4): 538-547.
19. Aleke, CG; Ibuo, JC & Obiora, DN. 2018. Application of electrical resistivity method in estimating geohydraulic properties of a sandy hydrolithofacies: a case study of Ajali Sandstone in Ninth Mile, Enugu State, Nigeria. *Arabian Journal of Geosciences,* 11 (1): 322. DOI: https://doi. org/10.1007/s1251 7-018-3638-8.1.
20. Putranto, TT; Santi, N; Dian, A; Widiarso, D.A & Dimas, PD. 2018. Application of aquifer vulnerability index (AVI) method to assess groundwater vulnerability to contamination in Semarang Urban Area. In: *MATEC Web of Conferences Series,* 159: 1-36.
21. Ishola, SA. 2019. Characterization of groundwater resource potentials using integrated techniques in selected communities within Ewekoro Local Government Area South-West Nigeria. *Department of Physics, FUNAAB Ph.D. Thesis.*
22. Loke MH. 2009. Electrical imaging surveys for environmental and engineering studies, a guide to 2D and 3D surveys. Workshop Held in USM: 22-23.
23. Ishola SA; Makinde V; Gbadebo AM; Mustapha AO & Orebiyi EA. 2021. Quality assessment of groundwater system in Itori community of Ewekoro Local Government Area, South-West Nigeria.*Science and Technology (SCI & TECH*) Multidisciplinary Engineering Science Studies, 5 (12): 2-7. http://scitechpub.org/index.php/vol-5-issue-12-December-2021.
24. Bashir, IY; Izham, MY; & Main R. 2014. Vertical Electrical sounding investigation of aquifer composition and its potential to yield groundwater in some selected towns in Bida Basin of North Central Nigeria. *Journal of Geography and Geol*ogy, 6(1): 60–69.
25. Obaje NG. 2009. *Geology and Mineral Resources of Nigeria*. 120. Springer, Berlin.
26. Ushie, F; Harry, T; & Affiah, U. 2014. Reserve estimation from geoelectrical sounding of the ewekoro limestone at Papalanto, Ogun State, Nigeria.*Journal of Energy Technologies and Policy*, 4(5): 28.
27. Billman, HG. 1992. Offshore stratigraphy and paleontology of the dahomey (benin) embayment. West Africa, *1st. NAPE Bull*, 7 (2): 121-130.
28. Stempvoort, DV; Ewert, L & Wassenaar, L. 1993. Aquifer Vulnerability Index: A GIS-compatible method for groundwater vulnerability mapping, *Canada Water Resources Journal*, 18 (1): 25-37.
29. Gemail, KS; El-Shishtawy, AM; El-Alfy, M; Ghoneim, MF, & Abdel-bary, MH. 2011. Assessment of aquifer vulnerability to industrial waste water using resistivity measurements, a case study, along El-Gharbyia main drain, Nile Delta, Egypt. *Journal of Applied Geophysics,* 75 (1): 140-150.
30. Heigold, PC; Gilkeson, RH; Cartwright K & Reed, PC. 1979. Aquifer transmissivity from surficial electrical methods. *Groundwater,* 17 (4): 338-345.
31. Worthington, RH; Smart, C & Ruland, W. 2002. Assessment of groundwater velocities to the municipal wells at Walkerton. In: Stolle D, Piggott AR, Crowder J.J (eds) *Ground and Water: Theory to Practice*. Proceedings of the 55th Canadian Geotechnical and 3rd Joint IAH-CNC and CGS Groundwater Specialty Conferences, Niagara Falls, Ontario, October 20-23, 2002.
32. Omosuyi, GO. 2010. Geoelectric assessment of groundwater prospect and nulnerability of overburden aquifers at Idanre, Southwestern Nigeria. *Ozean Journal of Applied Sciences*, 3 (1): 9-28.

33. Oyedele, KF & Adeyemo, AO. 2001. Surface electrical resistivity measurement in the characterization of groundwater potentials of the typical basement terrain, Northern Nigeria. *African Journal of Environmental Studies*, 2 (1): 52-54.
34. Aizebeokhai, AP, Olayinka, AI & Singh, VS. 2010b. Application of 2D and 3D geoelectrical resistivity imaging for engineering site investigation in a crystalline basement terrain, southwestern Nigeria. *Environ Earth Sci*, 61 (7): 1481-1492.

35. Olabode, SO & Muhammed, MZ. 2016. Depositional facies and sequence stratigraphic study in parts of Benin (Dahomey) Basin, SW Nigeria. Implications on the Re-Interpretation of Tertiary Sedimentary Successions. *International Journal of Geosciences*, 7 (1): 210-228. https://www.scirp.org. Retrieved on June 2nd, 2025.

36. Badmus, BS & Olatinsu OB. 2009. Geoelectric mapping and characterization of limestone deposits of Ewekoro formation, Southwestern Nigeria, *Journal of Geology and Mining Research*. 1 (1): 8-18. http://www.academicjournals.org/jgmr.

37. Akinyemi, LP; Odunaike, RK & Adeyeloja A. 2015. Physicochemical characterization of limestone deposits at Ewekoro, Ogun State, South-West of Nigeria and the *Environment Impact*. *Journal of Environment and Earth Science*, 5 (1): 18-36. www.iiste.org.
38. Oladosu, YC &Ogundipe OY. 2017. Micropaleotological studies of Ewekoro Sediments Southwestern Nigeria. *Journal of Geology and Geophysics*, 6 (1): 280. https://doi.org.10.4172/2381-8719.1000280.
39. Majolagbe, AO; Yusuf, KA &Duru, AE. 2013. Characterisation n Environmental Media: A Case Study of Cement Production Area, Ewekoro, Southwest, Nigeria. *European Scientific Journal*, 3 (1): 1857-7431.
40. Aizebeokhai, AP & Oyebanjo, OA. 2013. Application of vertical electrical soundings to characterize aquifer potential in Ota, Southwestern Nigeria. *International Journal of Physical Sciences*, 8 (46): 2077-2085.
41. Aizebeokhai, AP & Oyeyemi, KD. 2014. The use of multiple-gradient array forgeo-electrical resistivity and induced polarization imaging. *Journal of Applied Geophysics*, 12 (1): 10-12. http:// http://10.1016/J.Jappgeo.2014.10.023 .

42. Ward, SH & Hohmann, GW. 1987. Electromagnetic theory for geophysical applications. In: Nabighian MN (Ed.), Electromagnetic methods in applied geophysics, Investigations in Geophysical Series. *Society of Exploration Geophysics*, 1 (1): 131-312.

43. Ajayi, CO. & Hassan. 1990. The delineation of aquifer overlying the basement complex in the western Part of the Kubarni Basin of Zaria, Nigeria. *Journal of Mining and Geology*, 26 (1): 117-124.

44. Abiola, O; Enikanselu, PA & Oladapo, MI. 2009. Groundwater potential and aquifer protective capacity of overburden units in Ado-Ekiti, Southwestern Nigeria. *International Journal of Physical Sciences*, 4 (3): 120-132.

45. Aizebeokhai AP, Alile OM, Kayode JS, & Okonkwo FC. 2010a. Geophysical investigation of some flood prone areas in Ota, south- western Nigeria.American-*Eurasian Journal of Science Research*. 5 (4): 216-229.

46. Omosuyi, GO; Adegoke, AO & Adelusi, AO. 2008. Interpretation of electromagnetic and geoelectrical sounding data for groundwater resources around Obanla-Obakekere, near Akure, Southwestern Nigeria. *The Pacific Journal of Science and Technology*, 9 (2): 508-525.

Data availability

The data that support the findings of this study are available from the authors upon reasonable request.

Declaration of competing interest

The authors declare that they have no competing financial interests or personal relationships that could have appeared to influence the work reported in this paper.

Use of AI tools declaration

The authors declare that they have not used Artificial Intelligence (AI) tools in the creation of this article.